

Field emission properties of patterned carbon nanotube cathodes prepared by cold-pressing method

Ao Xia^a, Yunpeng Liu^{a,b,*}, Sheng Lai^a, Kang Wang^a, Xiushan Wang^a, Hao Yu^a, Xiaobin Tang^{a,b,*}

^a Department of Nuclear Science and Technology, Nanjing University of Aeronautics and Astronautics, Nanjing 210016, China

^b Key Laboratory of Advanced Nuclear Technology and Radiation Protection, Ministry of Industry and Information Technology, Nanjing 210016, China

ARTICLE INFO

Keywords:

Field emission
Cold-pressing method
Patterned cathode
Carbon nanotube

ABSTRACT

A method of preparing a patterned carbon nanotube (CNT) cathode via a cold-pressing method is used in this study. The patterned cathode exhibited a low turn-on field strength and no significant deterioration in electron emission property, and the effects of different cold-press pressures on the field emission property of the patterned cathode were studied. Experimental results showed that when the cold-press pressure is 50 MPa, the patterned cathode has excellent field emission properties with a current fluctuation of 3.19 % (initial current density of 1.5 mA/cm²), a low turn-on field of 0.77 V/μm, and an emission current density of 9.45 mA/cm² at an electric field of 2.17 V/μm. This study provides a feasible technical route for the low-cost and high-efficiency production of patterned cathode, which has broad application prospects.

1. Introduction

Field emission cathodes offer the advantages of normal operation at room temperature, a simple structure, and faster response speed [1,2]. Owing to their high aspect ratio and large tip curvature, carbon nanotubes (CNTs) can locally generate a strong electric field, which easily emits electrons and becomes an ideal material for developing field emission cathodes [1,3]. Consequently, CNT cathodes have shown broad application prospects in vacuum electronic devices such as X-ray sources [4], field emission displays [3,5], and light sources [6]. It should be noted that although CNT cathodes have potential in field emission displays and light sources, related research is still in the experimental or development stages, and no widely commercialized devices have yet been achieved.

Research indicates that the CNT density is crucial for field emission property. Nilsson et al. demonstrated via experimental and theoretical studies that excessive CNT density can cause a screening effect, which reduces the electric field at the emitter tips and consequently decreases the emission current [7]. Therefore, adjusting the CNT density can increase the emission current density. Both Kim et al. and Jiao et al. reported that the edges of patterned emission sites exhibit localized electric field enhancement, which can reduce the screening effect and increase the emission current [8,9]. The design of patterned emission

sites can effectively control the density of CNTs, thereby reducing the screening effect. In addition, Zhang et al. simulated the electric field distribution in a triode structure, and the results showed that the electric field intensity at the edge of the patterned emission point was significantly higher than that in other regions [10]. According to the simulation results, we infer that the field emission mainly comes from the edge of patterned emission points.

Currently, the main methods for preparing patterned CNT field emitters include chemical vapor deposition (CVD) [9,11,12], screen printing [3,13], and electrophoretic deposition [14]. In 2005, Zhao et al. obtained patterned CNT emitters on a silicon substrate using electrophoretic deposition, achieving a current density of 30 mA/cm² under an electric field of 8 V/μm [14]. In 2006, Kwon et al. prepared square-type and line-type CNT emitters via screen printing. The experimental results revealed that the square-type CNT emitters presented a higher emission current and more stable emission property, with an emission current density of 243 μA/cm² at an electric field of 10 V/μm [3]. In 2008, Liao et al. prepared a large-area, non-patterned CNT cathode via screen printing. The experimental results show that under a single pulse electric field with an electric field of 16.7 V/μm, the max emission current of the screen printing cathode is 1.95 kA [15]. In 2015, Wei et al. used microwave plasma-enhanced CVD to grow patterned CNT arrays as electron emitters, reaching a maximum current density of 4.5 A/cm² [16]. In

* Corresponding authors at: Department of Nuclear Science and Technology, Nanjing University of Aeronautics and Astronautics, Nanjing 210016, China.

E-mail addresses: liuyyp@nuaa.edu.cn (Y. Liu), tangxiaobin@nuaa.edu.cn (X. Tang).

<https://doi.org/10.1016/j.diamond.2025.112059>

Received 28 October 2024; Received in revised form 27 January 2025; Accepted 29 January 2025

Available online 30 January 2025

0925-9635/© 2025 Elsevier B.V. All rights are reserved, including those for text and data mining, AI training, and similar technologies.

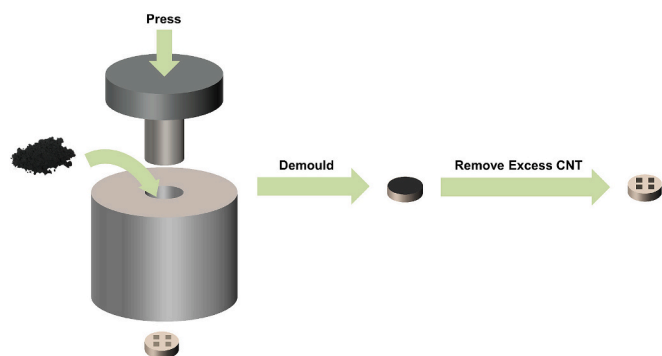


Fig. 1. Schematic of the preparation of a patterned cathode by the cold-pressing method.

2019, Kong et al. grew nonpatterned and stripe-patterned CNT emitters on alloy substrates via CVD. Their experiments revealed that the emission current of the patterned emitter was greater than that of the non-patterned emitter at the same gate voltage [17]. In 2023, Chen et al. achieved high field emission from patterned cold cathodes by screen-printing CNT paste onto small-hole-patterned substrates. The CNT cold cathodes exhibited an emission current of up to 45 mA at an electric field of $7 \text{ V}/\mu\text{m}$ [13].

Although the CVD method has excellent properties in the preparation of patterned field emitters, it is complex and costly [9]. In contrast, screen-printing and electrophoretic deposition are favored for their low cost and large-area patterning capabilities [13,18]. However, the organic solvents and binders commonly used in screen printing often have poor conductivity, which increases the contact resistance between the CNTs and the substrate and potentially buries the CNTs, leading to degradation of the field emission property of the cathode [19]. Similarly, electrophoretic deposition requires high-quality suspensions, and an excessive amount of surfactant can lead to CNT entanglement and agglomeration, which will adversely affect the field emission property [20]. For the issues associated with CVD, screen-printing and electrophoretic deposition methods to be addressed, this study proposes a low-cost cold-pressing method for preparing patterned cathodes by using only CNTs without auxiliary materials. Additionally, a diode device was designed and built to evaluate the field emission property.

2. Experimental details

2.1. Preparation method

In this study, industrial-grade multiwalled CNTs (MWCNTs) with outer diameters of $<10 \text{ nm}$ and lengths of $5\text{--}15 \mu\text{m}$ were used as electron emitters. Square hole patterns were fabricated on the stainless steel substrate via a laser etching method. Then, the substrates were ultrasonically cleaned in anhydrous ethanol for 10 min and dried at 70°C for 20 min to reduce the contact resistance between the CNTs and the substrate. Then, the CNTs were pressed onto the patterned substrates, followed by mechanical activation treatment.

Fig. 1 shows the procedure for preparing patterned cathodes via the cold-pressing method. First, a cleaned stainless steel substrate with square hole patterns, CNTs, and an upper indenter were placed in a cold-press mold. Then, different pressures were applied to the upper indenter via a tablet press (MCS-30), and the samples were demoulded after maintaining each pressure for 5 min. A razor was then used to remove CNTs from the nonpatterned areas of the substrates with square hole patterns to obtain the patterned cathodes. Finally, the patterned cathodes were mechanically activated via a rubber roller, and a tape was used to remove contaminants outside the patterned emission sites on the patterned cathode surface. The patterned cathodes prepared via the cold-pressing method are denoted P-X, where $X = 30, 50, 100, 150$, or

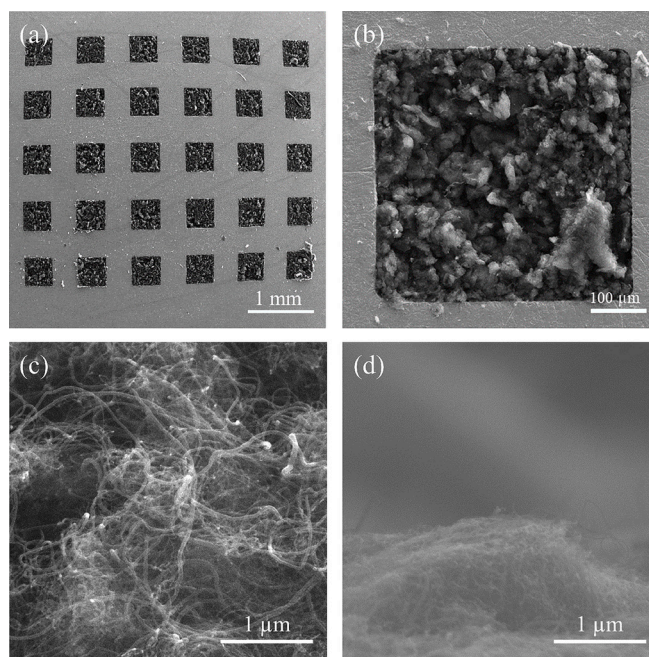


Fig. 2. (a) Image of a stainless steel substrate with square hole patterns, (b) patterned emission sites, (c) top-view FIB-SEM image of the patterned cathode, and (d) side-view FIB-SEM image of the patterned cathode.

200 MPa, which represents the applied pressure.

2.2. Characterization and measurement methods

The microstructure of the cold-pressed CNTs was characterized via focused ion beam scanning electron microscopy (FIB-SEM, LYRA3 GMU). A laser Raman spectrometer (LabRAM HR Evolution, excitation wavelength of 532 nm) was used to obtain Raman spectra of the cold-pressed CNTs. The adhesion of cold-press CNT films to the substrate was evaluated using a micron scratch tester. Field emission property tests were conducted in a dynamic vacuum system with an initial vacuum of $1 \times 10^{-7} \text{ Pa}$ [2], using a homemade diode device with a copper sheet as the anode, and the distance between the patterned cathode and the anode was about $470 \mu\text{m}$.

A DC high-voltage power supply was used to apply voltage to the anode, and the current-voltage (I - V) properties of the patterned cathode were measured with a digital multimeter. A 200Ω resistor was connected in series between the cathode and the multimeter to protect the multimeter. After the I - V properties were measured, the vacuum was restored to $1 \times 10^{-7} \text{ Pa}$, and the emission stability of the cathode was evaluated with a data acquisition card (DAM-3158A).

3. Results and discussion

3.1. Property of patterned cathodes

Fig. 2(a) and (b) shows FIB-SEM images of the patterned cathode at different magnifications. Fig. 2(a) shows the surface morphology of the substrate, which was etched with regular square hole patterns via a laser. These patterns have a side length of $440 \mu\text{m}$ with a tolerance of $\pm 5\%$, a spacing of approximately $400 \mu\text{m}$, and a depth of approximately $200 \mu\text{m}$. The cathode surface contains a total of 35 square hole patterns, with a total emission area of 0.06776 cm^2 . The square holes were filled with CNTs via the cold-pressing method, as shown in Fig. 2(b), forming patterned emission sites. Some residual CNTs were observed outside the patterned emission areas. The top-view and side-view FIB-SEM images of the patterned cathode are shown in Fig. 2(c) and (d). In particular,

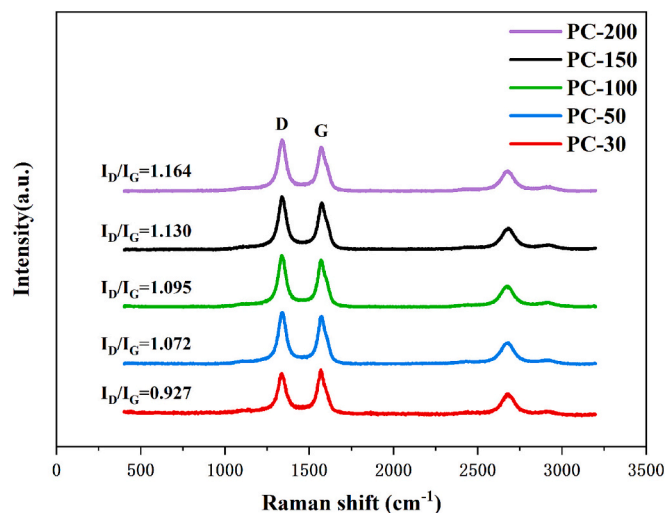


Fig. 3. Raman spectra of patterned cathodes prepared with different cold-press pressures.

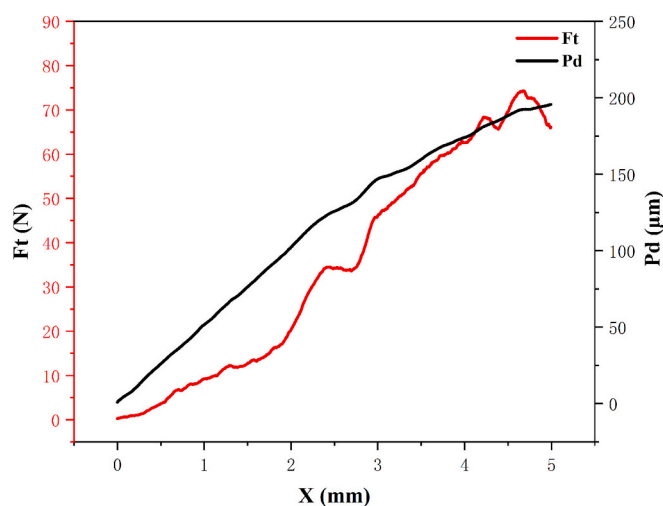


Fig. 4. Variation of friction and penetration depth with scratch displacement.

Fig. 2(c) shows the surface of the patterned cathode, where the CNTs are densely entangled with almost no impurities, and the white dots are the protruding ends of the CNTs. Fig. 2(d) shows that the cold-pressing method compacts the arrangement of the CNTs. After mechanical activation treatment, the CNTs exhibit an overall upward inclined orientation.

The crystallinity of the CNT emitters prepared under different cold-

press pressures was evaluated via Raman spectroscopy (Fig. 3). The two prominent peaks in the Raman spectrum are the D peak ($\sim 1340 \text{ cm}^{-1}$) and the G peak ($\sim 1570 \text{ cm}^{-1}$). The D peak arises from the radial respiration mode vibration of the hexagonal carbon ring, whereas the G peak originates from the stretching of sp^2 -hybridized C=C bonds [21]. The intensity ratio of the D peak to the G peak (I_D/I_G) is generally used to measure the crystallinity of CNTs, and a smaller ratio indicates better structural perfection of the CNTs [22]. Here, the I_D/I_G value increases from 0.927 to 1.164 as the cold-press pressure increases from 30 MPa to 200 MPa, indicating a decrease in structural perfection with increasing cold-press pressure. This is due to the increasing cold-press pressure exerted on the CNTs, leading to structural defects such as deformation, fractures, or dislocations of the tube wall. These structural defects result in an increased D peak intensity, causing the I_D/I_G value to rise and the structural perfection to decrease.

The adhesion between the CNT film and the substrate was characterized through micron scratch test of a non-patterned cathode prepared under a cold-press pressure of 50 MPa. As shown in Fig. 4, the frictional force gradually increases with the scratch position, reflecting an increase in the frictional resistance between the CNT film and the substrate. At a position of approximately 4.29 mm, a significant fluctuation is observed in the friction curve, indicating that the CNT film may experience local rupture or detachment. The penetration depth increases linearly with position, which is consistent with the scratch loading process, indicating that the carbon nanotube film has not undergone large-scale detachment. The experimental results show that the adhesion between the cold-pressed CNT film and the substrate is average. Therefore, the adhesion force between the cold-pressed CNT film and the substrate can be attributed to the combined effects of electrostatic interactions, the high specific surface area of CNTs, and van der Waals forces.

In the field of field emission, the Fowler-Nordheim (FN) plot is commonly used to analyze I - V or J - E data. In 2019, Richard G. Forbes proposed that plotting I - V data as Murphy-Good (MG) plots allows for a more accurate extraction of emitter characterization parameters [23]. To calculate the field enhancement factor more accurately, MG plots are used in this paper for data analysis. Meanwhile, in order to provide a more intuitive representation of the field emission properties, current density, turn-on field (E_{on}) and threshold field (E_{th}) are used for characterization. Therefore, in the following sections, current and voltage are converted to current density and electric field intensity.

The I - V curves and the corresponding MG plots of the patterned cathode prepared under different cold-press pressures are shown in Fig. 5. The applied electric fields required to generate emission current densities of $10 \mu\text{A}/\text{cm}^2$ and $1 \text{ mA}/\text{cm}^2$ are defined as the E_{on} and the E_{th} , respectively.

As shown in Fig. 5(a), P-50 achieves electron emission at a lower electric field intensity, with $E_{on} \approx 0.77 \text{ V}/\mu\text{m}$ and $E_{th} \approx 1.42 \text{ V}/\mu\text{m}$. For P-30, P-100, P-150, and P-200, E_{on} increases to 1.25, 0.91, 1.00, and $1.40 \text{ V}/\mu\text{m}$, respectively, and E_{th} also increases to 1.86, 1.68, 1.84, and $2.78 \text{ V}/\mu\text{m}$, respectively. The emission current density of P-50 reaches

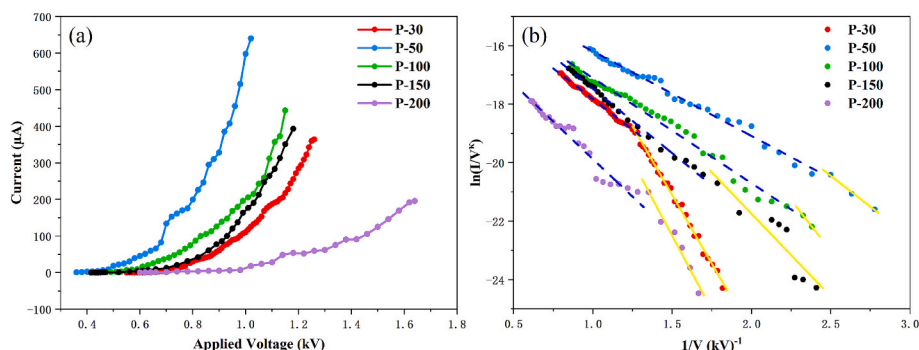


Fig. 5. (a) I - V curves and (b) corresponding $\ln(I/V^2)$ vs $1/V$ curves of patterned cathodes prepared under different cold-press pressures.

9.45 mA/cm² in an electric field of 2.17 V/μm, whereas those of P-30, P-100, P-150, and P-200 reaches 5.37, 6.36, 5.8, and 2.88 mA/cm² in electric fields of 2.57, 2.45, 2.51, and 3.48 V/μm, respectively. As the cold-press pressure increases, the CNTs at the patterned emission sites become more tightly packed and tend to tilt (Fig. S1). At lower cold-press pressures, the number of emission sites is higher, which causes a screening effect, leading to a low emission current density at the same electric field. When the cold-press pressure reaches approximately 50 MPa, the number of emission sites is moderate, reducing the screening effect and increasing the emission current density. However, with further increases of the cold-press pressure, the compaction of the CNT leads to a further decrease in the number of emission sites, resulting in a gradual decrease in the emission current density at the same electric field. In addition, as the applied electric field gradually increased, residual CNTs outside the emission sites and weakly adhered CNTs at the emission sites caused fluctuations in the emission current density.

The FN equation, widely used for calculating the field enhancement factor, is expressed as follows [24]:

$$J = \frac{A\beta^2 E^2}{\phi} \exp\left(-\frac{B\phi^3}{\beta E}\right), \quad (1)$$

where J is the field emission current density, β is the field enhancement factor, ϕ is the work function of the CNTs (~4.95 eV for MWCNTs) [25], E is the electric field strength, and A and B are constants ($A = 1.56 \times 10^{-6} \text{ A}\cdot\text{eV}\cdot\text{V}^{-2}$, $B = 6.83 \times 10^3 \text{ V}\cdot\text{eV}^{-3/2}\cdot\mu\text{m}^{-1}$). According to Eq. (1), the field enhancement factor can be deduced as follows:

$$\beta = -\frac{B\phi^{3/2}}{k} \quad (2)$$

where k is the slope of the FN plot. According to the slope of each FN curve, the field enhancement factors of P-30, P-50, P-100, P-150, and P-200 are 6196, 14,139, 11,380, 9668, and 8284, respectively.

In 1956, Murphy and Good proposed an improved field electron emission theory based on the work of Burgess et al. [26,27]. This theory assumes that tunneling occurs through a planar image-rounded tunneling barrier, which is now referred to as the ‘‘Schottky-Nordheim (SN) barrier.’’ The fundamental equation of the MG theory is as follows [23,28]:

$$I_m(f_c) \approx A_f^{SN} \cdot \theta \exp(\eta) \cdot f_c^k \cdot \exp\left(-\frac{\eta}{f_c}\right), \quad (3)$$

$$k = 2 - \frac{\eta}{6}, \quad (4)$$

$$\theta(\phi) = A c_s^{-4} \phi^3, \quad (5)$$

where $ASNf$ is the effective emission area, f_c is f_c value, κ is the voltage exponent, and c_s is the ‘‘Schottky constant’’. The formulas for c_s and η are as follows [23,29]:

$$c_s = \sqrt{\frac{e^3}{4\pi\epsilon_0}}, \quad (6)$$

$$\eta \approx 9.8362 \left(\frac{eV}{\phi}\right)^{1/2}, \quad (7)$$

where e is the elementary charge, and ϵ_0 is the permittivity of free space.

According to Eq. (3), the extraction equation for the field enhancement factor is given by:

$$\beta^{extr} = -\frac{s_t B \phi^{3/2} d}{k_{slope}}, \quad (8)$$

where s_t is a fitting value ($s_t \approx 0.95$), d is the distance between the anode and the emitter, and k_{slope} is the slope of the MG plot.

Table 1

Examining the variation and acceptability of field enhancement factor based on the field emission properties of the cold-pressed cathodes.

Type	d (μm)	β_{extr} H	f^{extr} range (Remark)	β_{extr} L	f^{extr} range (Remark)
P-30	490	8345	0.791 to 1.261 (Unacceptable)	3728	0.246 to 0.349 (Acceptable)
P-50	470	11,597	0.609 to 1.479 (Unacceptable)	7947	0.358 to 0.398 (Acceptable)
P-100	470	9341	0.526 to 1.343 (Unacceptable)	4875	0.256 to 0.262 (Acceptable)
P-150	470	7621	0.562 to 1.12 (Unacceptable)	5935	0.308 to 0.416 (Acceptable)
P-200	470	6540	0.638 to 1.341 (Unacceptable)	3301	0.248 to 0.305 (Acceptable)

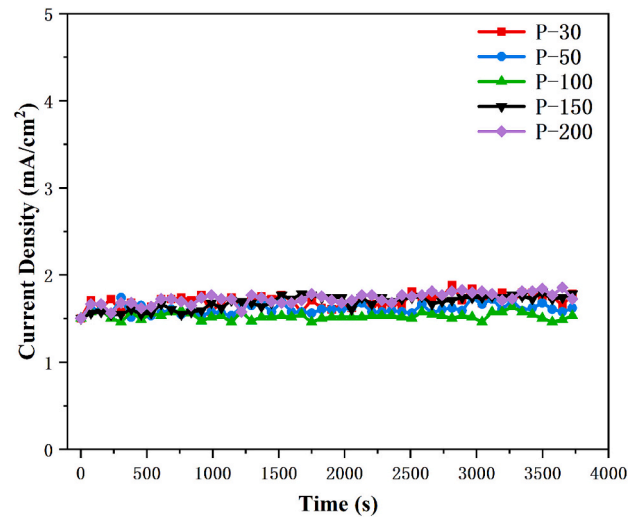


Fig. 6. Field emission stability of patterned cathodes prepared by different cold-press pressures.

In experiments, the practical emission situations often exhibit unorthodox characteristics, which can lead to spurious results using Eq. (2). To address this issue, Richard G. Forbes proposed the ‘‘orthodoxy test’’, which assumes the tunnel barrier to be an SN barrier, selects an appropriate I - V data, and then calculates the field enhancement factor using Eq. (8). The equation for calculating the f^{extr} value used in this testing method is as follows [30]:

$$f^{extr} = -\frac{-s_t \eta}{k_{slope} \times (V^{-1})}, \quad (9)$$

where η is the dimensionless scaling parameter in the exponent of scaled forms of FN-type equations based on the SN barrier. When the $\phi \approx 4.95$ eV, the range of f^{extr} is between 0.14 and 0.43 [30], and the emission is considered ‘‘orthodox’’. As shown in Table 1, the experimental data passed the test in the low electric field region and failed in the high electric field region, indicating that the field enhancement factor in the high electric field region is overestimated.

After the I - V property test, the patterned cathode was subjected to electrical aging for 1 h at an initial current density of approximately 1.5 mA/cm² to remove poorly adherent CNTs from the surface of the patterned cathode and further activate the CNTs. During this process, a slight increase in current density was observed. The current density was maintained at 1.5 mA/cm² by adjusting the voltage, followed by a field emission stability test. The test results are shown in Fig. 6. The current fluctuation was calculated according to Eq. (10) [31].

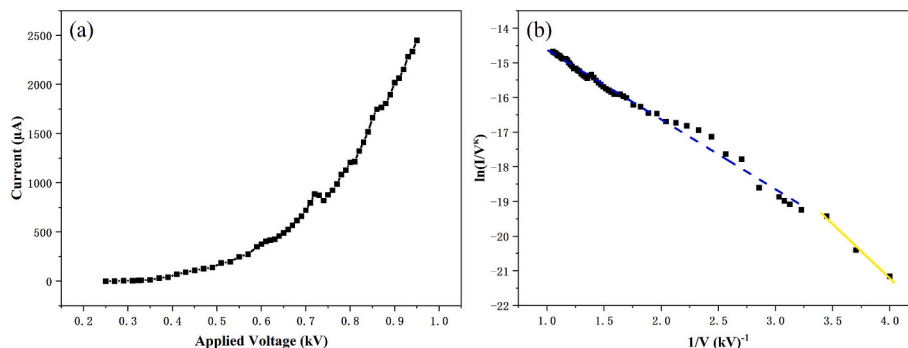


Fig. 7. I – V curves (a) and $\ln(I/V^{0.75})$ vs $1/V$ curves (b) of the nonpatterned cathode.

$$\delta_J = \frac{\sum_{i=1}^N |J_i - \bar{J}|}{N\bar{J}} \times 100\%, \quad (10)$$

where J_i is the current density of each measurement point, \bar{J} is the average current density, and N represents the total number of measurement points. The current fluctuations of P-30, P-50, P-100, P-150, and P-200 are 3.2 %, 3.19 %, 2.46 %, 3.87 % and 3.11 %, respectively. These fluctuations are all < 4 %, indicating that the patterned cathodes achieve stable field emission property. The patterned cathode prepared at 50 MPa exhibited superior electron emission property and stability, which is attributed to the good interfacial contact of the patterned emission sites [13], and the low screening effect caused by the patterned design.

3.2. Comparison of patterned and non-patterned cathodes

A nonpatterned cathode was prepared at a pressure of 50 MPa (Fig. S2) to confirm whether the patterned design can weaken the screening effect. The area of the non-patterned cathode is about 0.78540 cm^2 and the spacing between the non-patterned cathode and the anode is $420 \text{ }\mu\text{m}$. Given the low cold-press pressure, the CNTs on the nonpatterned cathode were loosely arranged and generally upright (Fig. S3). Fig. 7 shows the I – V curve and the corresponding MG plot of the nonpatterned cathode. Owing to vacuum limitations, the maximum emission current density recorded was within 4 mA/cm^2 . The E_{on} of the nonpatterned cathode is approximately $0.77 \text{ V}/\mu\text{m}$, and the E_{th} is approximately $1.69 \text{ V}/\mu\text{m}$. At an electric field of $2.26 \text{ V}/\mu\text{m}$, the emission current density reaches 3.12 mA/cm^2 . By contrast, when the emission current density of the patterned cathode prepared under the same cold-press pressure reached 3.33 mA/cm^2 , the electric field was $1.74 \text{ V}/\mu\text{m}$. According to Eq. (2), the field enhancement factor of the nonpatterned cathode is calculated to be 18,527, which is significantly greater than that of the patterned cathode prepared under the same cold pressing pressure. The f^{extr} of the non-patterned cathode was calculated using the Eq. (9). In the high electric field region, $0.646 < f^{\text{extr}} < 1.981$, failing the orthodoxy test; while in the low electric field region, $0.336 < f^{\text{extr}} < 0.389$, passing the orthodoxy test. The field enhancement factor

in the low electric field region is 9595. As shown in the FIB–SEM images in Figs. S1(a) and S3, the CNTs in the nonpatterned cathode are more loosely arranged, which reduces the screening effect and thus results in a higher field enhancement factor [7]. However, the patterned design effectively reduces the screening effects at each emission site, leading to a higher emission current density for the patterned cathode than for the nonpatterned cathode under the same applied electric field.

3.3. Patterned CNT cathodes with different preparation methods

The approach of using patterned CNT cathodes prepared by CVD was compared with screen-printing methods to elucidate the field emission properties of cold-pressed patterned CNT cathodes. Table 2 summarizes E_{on} , the current density, and the field enhancement factor. To facilitate comparison with the results in the extensive existing literature, the field enhancement factors in Table 2 were calculated based on Eq. (2). The results indicate that the cold-pressed patterned CNT cathode has a lower E_{on} and a higher field enhancement factor, whereas its maximum current density still requires further improvement compared with the values reported in the literature.

4. Conclusion

This study successfully fabricated patterned CNT cathodes via a cold-pressing method, reducing preparation costs and simplifying the process. The patterned cathode prepared at 50 MPa cold-press pressure showed the best electron emission property, with an E_{on} of approximately $0.77 \text{ V}/\mu\text{m}$ and an emission current density of 9.45 mA/cm^2 at an electric field of $2.17 \text{ V}/\mu\text{m}$. Future research could further optimize the geometric structure and cold-pressing parameters of the cathode to increase its potential applications in vacuum electronic devices.

Supplementary data to this article can be found online at <https://doi.org/10.1016/j.diamond.2025.112059>.

CRedit authorship contribution statement

Ao Xia: Writing – review & editing, Writing – original draft, Investigation, Formal analysis, Data curation. Yunpeng Liu: Writing – review

Table 2

Comparison of the field emission properties of patterned CNT cathodes prepared via different methods.

Type	Method	E_{on} (V/ μm)	J_{max} (mA/ cm^2)/ E (V/ μm)	Stability (%)/ Time(h)	β	Reference
CNTs	TCVD	2 (100 $\mu\text{A}/\text{cm}^2$)	14.6/4.8	4.1 % fluctuation/6	5937	[11]
CNTs	DC-PECVD	3 (10 $\mu\text{A}/\text{cm}^2$)	2.88/4.53		2821	[32]
Cu-VACNTs	PECVD	2.33 (10 $\mu\text{A}/\text{cm}^2$)	$\sim 20.5/4.5$	~ 26 % decline/5	2037	[33]
MWCNTs	Screen-printing	0.58 (10 $\mu\text{A}/\text{cm}^2$)	$\sim 109/2.2$	50 % decline/ ~ 4	8710	[34]
CNTs	Screen-printing	0.85 (10 $\mu\text{A}/\text{cm}^2$)	$\sim 3.5/2.5$	9 % decline/2	14,963	[6]
SWCNTs	Screen-printing	2.3 (1 mA/ cm^2)	643/7		2113	[13]
MWCNTs	Cold-pressing	0.77 (10 $\mu\text{A}/\text{cm}^2$)	9.45/2.17	3.19 % fluctuation/ ~ 1	14,139	This work

& editing, Supervision, Resources, Funding acquisition. **Sheng Lai:** Writing – review & editing, Investigation, Formal analysis. **Kang Wang:** Writing – review & editing, Data curation. **Xiushan Wang:** Writing – review & editing, Investigation. **Hao Yu:** Writing – review & editing. **Xiaobin Tang:** Writing – review & editing, Supervision, Resources.

Declaration of competing interest

The authors declare that they have no known competing financial interests or personal relationships that could have appeared to influence the work reported in this paper.

Acknowledgments

This work was supported by the National Natural Science Foundation of China (Grant No. 12375256).

Data availability

Data will be made available on request.

References

- [1] S. Zhou, K. Chen, M.T. Cole, Z. Li, J. Chen, C. Li, Q. Dai, Ultrafast field-emission electron sources based on nanomaterials, *Adv. Mater.* 31 (2019) 1805845, <https://doi.org/10.1002/adma.201805845>.
- [2] S. Lai, X. Tang, Y. Liu, J. Mu, Z. Feng, K. Miao, X-ray high frequency pulse emission characteristic and application of CNT cold cathode X-ray source cathode X-ray source, *Nanotechnology* 33 (2022) 075201, <https://doi.org/10.1088/1361-6528/ac378b>.
- [3] S.J. Kwon, S.H. Lee, Field emission characteristics depending on emitter patterns of a screen-printed carbon nanotube field emission array, *Jpn. J. Appl. Phys.* 45 (2006) 355–358, <https://doi.org/10.1143/JJAP.45.355>.
- [4] K. Miao, Y. Liu, S. Lai, J. Yin, F. Xiong, X. Dong, X. Tang, Emission characteristics of pulse CNT cold cathode X-ray source combined with channel electron multiplier, *Appl. Radiat. Isot.* 206 (2024) 111243, <https://doi.org/10.1016/j.apradiso.2024.111243>.
- [5] X.Q. Li, Fabrication research on the double cathode-conducting-layer for diode field emission display with CNT emitters, *Appl. Mech. Mater.* 174–177 (2012) 588–591, <https://doi.org/10.4028/www.scientific.net/AMM.174-177.588>.
- [6] M.-J. Youh, C.-L. Huang, Y.-L. Wang, L.-M. Chiang, Y.-Y. Li, Development of a high-brightness field-emission lighting device with ITO electrode, *Vacuum* 181 (2020) 109733, <https://doi.org/10.1016/j.vacuum.2020.109733>.
- [7] L. Nilsson, O. Groening, C. Emmenegger, O. Kuettel, E. Schaller, L. Schlapbach, H. Kind, J.-M. Bonard, K. Kern, Scanning field emission from patterned carbon nanotube films, *Appl. Phys. Lett.* 76 (2000) 2071–2073, <https://doi.org/10.1063/1.126258>.
- [8] N.S. Lee, D.S. Chung, I.T. Han, J.H. Kang, Y.S. Choi, H.Y. Kim, S.H. Park, Y.W. Jin, W.K. Yi, M.J. Yun, J.E. Jung, C.J. Lee, J.H. You, S.H. Jo, C.G. Lee, J.M. Kim, Application of carbon nanotubes to field emission displays, *Diam. Relat. Mater.* 10 (2001) 265–270, [https://doi.org/10.1016/S0925-9635\(00\)00478-7](https://doi.org/10.1016/S0925-9635(00)00478-7).
- [9] D. McClain, J. Wu, N. Tavan, J. Jiao, C.M. McCarter, R.F. Richards, S. Mesarovic, C. D. Richards, D.F. Bahr, Electrostatic shielding in patterned carbon nanotube field emission arrays, *J. Phys. Chem. C* 111 (2007) 7514–7520, <https://doi.org/10.1021/jp067868h>.
- [10] Y. Zhang, T. Lin, X. Zeng, X. Zhou, T. Guo, Fabrication and field emission characteristics of a novel planar-gate electron source with patterned carbon nanotubes for backlight units, *J. Semicond.* 34 (2013) 064005, <https://doi.org/10.1088/1674-4926/34/6/064005>.
- [11] G. Kumar, H. Gupta, S. Ghosh, P. Srivastava, Highly enhanced field emission from vertically aligned carbon nanotubes grown on a patterned substrate via non-lithographic method, *Phys. E Low-Dimens. Syst. Nanostructures* 135 (2022) 114946, <https://doi.org/10.1016/j.physe.2021.114946>.
- [12] D.V. Gorodetskiy, A.G. Kurenaya, A.V. Gusev'nikov, K.I. Baskakova, D.A. Smirnov, V.E. Arkhipov, L.G. Bulusheva, A.V. Okotrub, Laser beam patterning of carbon nanotube arrays for the work of electron field emitters in technical vacuum, *Mater. Sci. Eng. B* 262 (2020) 114691, <https://doi.org/10.1016/j.mseb.2020.114691>.
- [13] J. Chen, X. Chang, G. Ma, Y. Zhu, B. Yang, Y. Zhao, J. Chen, Y. Li, Boosting field electron emission of carbon nanotubes through small-hole-patterning design of the substrate, *J. Phys. D: Appl. Phys.* 57 (2024) 095302, <https://doi.org/10.1088/1361-6463/ad0e97>.
- [14] H. Zhao, H. Song, Z. Li, G. Yuan, Y. Jin, Electrophoretic deposition and field emission properties of patterned carbon nanotubes, *Appl. Surf. Sci.* 251 (2005) 242–244, <https://doi.org/10.1016/j.apsusc.2005.03.202>.
- [15] Liao Qing-Liang, Zhang Yue, Xia Lian-Sheng, Qi Jun-Jie, Huang Yun-Hua, Deng Zhan-Qiang, Gao Zhan-Jun, Cao Jia-Wei, Research on intense pulsed emission of screen-printed carbon nanotube cathode, *Acta Phys. Sin.* 57 (2008) 2328, <https://wulixb.iphy.ac.cn/article/doi/10.7498/aps.57.2328>.
- [16] W. Wei, Yixiong Zheng, Xinyu Yuan, Yan Wang, Bing Liu, Xuebing Wang, Z. Chen, Carbon nanotube field emission electron gun for traveling-wave tube, in: 2015 IEEE Int. Vac. Electron. Conf. IVEC, IEEE, Beijing, China, 2015, pp. 1–2, <https://doi.org/10.1109/IVEC.2015.7224016>.
- [17] J. Lim, A.P. Gupta, S.J. Yeo, M. Kong, C.-G. Cho, S.H. Kim, J.S. Ahn, M. Mativenga, J. Ryu, Design and fabrication of CNT-based E-gun using stripe-patterned alloy substrate for X-ray applications, *IEEE Trans. Electron Devices* 66 (2019) 5301–5304, <https://doi.org/10.1109/TED.2019.2943870>.
- [18] M. Atiq Ur Rehman, Q. Chen, A. Braem, M.S.P. Shaffer, A.R. Boccacini, Electrophoretic deposition of carbon nanotubes: recent progress and remaining challenges, *Int. Mater. Rev.* 66 (2021) 533–562, <https://doi.org/10.1080/09506608.2020.1831299>.
- [19] H. Go, S.E. Han, H. Lee, C.J. Lee, Improved field emission properties of carbon nanotube paste emitters using an electrically conductive graphite binder, *ACS Appl. Electron. Mater.* 6 (2024) 3554–3562, <https://doi.org/10.1021/acsaelm.4c00313>.
- [20] S. Li, J. Yan, Y. Zhang, Y. Qin, Y. Zhang, S. Du, Comparative investigation of carbon nanotubes dispersion using surfactants: a molecular dynamics simulation and experimental study, *J. Mol. Liq.* 377 (2023) 121569, <https://doi.org/10.1016/j.molliq.2023.121569>.
- [21] V. Thapliyal, M.E. Alabdulkarim, D.R. Whelan, B. Mainali, J.L. Maxwell, A concise review of the Raman spectra of carbon allotropes, *Diam. Relat. Mater.* 127 (2022) 109180, <https://doi.org/10.1016/j.diamond.2022.109180>.
- [22] A. Jorio, E.H.M. Ferreira, M.V.O. Moutinho, F. Stavale, C.A. Achete, R.B. Capaz, Measuring disorder in graphene with the G and D bands, *Phys. Status Solidi B* 247 (2010) 2980–2982, <https://doi.org/10.1002/psbb.201000247>.
- [23] R.G. Forbes, The Murphy–Good plot: a better method of analysing field emission data, *R. Soc. Open Sci.* 6 (2019) 190912, <https://doi.org/10.1098/rsos.190912>.
- [24] R.H. Fowler, L. Nordheim, Electron emission in intense electric fields, *Proc. R. Soc. Lond.* 119 (1928) 173–181, <https://doi.org/10.1098/rspa.1928.0091>.
- [25] M. Shiraishi, M. Ata, Work function of carbon nanotubes, *Carbon* 39 (2001) 1913–1917, [https://doi.org/10.1016/S0008-6223\(00\)00322-5](https://doi.org/10.1016/S0008-6223(00)00322-5).
- [26] R.E. Burgess, H. Kroemer, J.M. Houston, Corrected values of Fowler-Nordheim field emission functions $v(y)$ and $s(y)$, *Phys. Rev.* 90 (1953) 515, <https://doi.org/10.1103/PhysRev.90.515>.
- [27] E.L. Murphy, R.H. Good, Thermionic emission, field emission, and the transition region, *Phys. Rev.* 102 (1956) 1464–1473, <https://doi.org/10.1103/PhysRev.102.1464>.
- [28] Y. Li, X. Li, Z. Qin, R. Wang, In-situ growth of carbon nanotubes oriented vertically on vertical graphene for field emission, *Vacuum* 228 (2024) 113537, <https://doi.org/10.1016/j.vacuum.2024.113537>.
- [29] A.G. Kolosko, S.V. Filippov, P.A. Romanov, E.O. Popov, R.G. Forbes, Real-time implementation of the “orthodoxy test” for conformity of current–voltage characteristics with classical field electron emission theory, *J. Vac. Sci. Technol. B Nanotechnol. Microelectron. Mater. Process. Meas. Phenom.* 34 (2016) 041802, <https://doi.org/10.1116/1.4946834>.
- [30] R.G. Forbes, Development of a simple quantitative test for lack of field emission orthodoxy, *Proc. R. Soc. Math. Phys. Eng. Sci.* 469 (2013) 20130271, <https://doi.org/10.1098/rspa.2013.0271>.
- [31] L. Wang, Y. Zhao, K. Zheng, J. She, S. Deng, N. Xu, J. Chen, Fabrication of large-area ZnO nanowire field emitter arrays by thermal oxidation for high-current application, *Appl. Surf. Sci.* 484 (2019) 966–974, <https://doi.org/10.1016/j.apsusc.2019.04.169>.
- [32] M.A. Chumak, A.V. Shchegolkov, E.O. Popov, S.V. Filippov, A.G. Kolosko, A. V. Shchegolkov, A.A. Babaev, Investigation of field emission properties of carbon nanotube arrays of different morphologies, *Nanomaterials* 14 (2024) 763, <https://doi.org/10.3390/nano14090763>.
- [33] C.E. Nwanno, A. Thapa, J. Watt, D. Simkins Bendayan, W. Li, Field emission properties of Cu-filled vertically aligned carbon nanotubes grown directly on thin Cu foils, *Nanomaterials* 14 (2024) 988, <https://doi.org/10.3390/nano14110988>.
- [34] S.J. Kim, S.A. Park, Y.-C. Kim, B.-K. Ju, Enhanced field emission properties from carbon nanotube emitters on the nanopatterned substrate, *J. Vac. Sci. Technol. B Nanotechnol. Microelectron. Mater. Process. Meas. Phenom.* 35 (2017) 011802, <https://doi.org/10.1116/1.4972119>.